Detection of brain abnormalities by *in vivo* MRI may serve as diagnostic and prognostic tests for acquired scoliosis in proprioception-deficient animal model of AIS

Ronen Blecher, MD, PhD; Eran Assaraf MD; Yossi Smorgick MD; Yoram Anekstein MD; Elazar Zelzer, PhD; Rod J. Oskouian, MD; Jens R. Chapman, MD; David Hanscom, MD; Robert A. Hart, MD and Inbal E. Biton, PhD

ABSTRACT

Efficient pre-scoliosis diagnostic and prognostic tools for AIS are currently lacking. Recently, we reported that mutant mice with a primary proprioceptive deficiency display an AIS-like acquired deformity. Here, we test the hypothesis that preceding brain abnormalities could predict the appearance of spinal deformity and its severity. By performing in-vivo brain MRI in our animal model of AIS, we show that specific and significant T2 signal brain abnormalities are detected prior to the development of scoliosis and may thus serve for early diagnosis and prognosis of the disease.

Introduction

Scoliosis, a 3-dimensional deformity of the spine, is one of the most prevalent pathologies affecting the musculoskeletal system (SRS, 2016). The undoubtedly most common subtype is the acquired form, usually presenting around sexual puberty in an otherwise healthy adolescents and for which a causative mechanism has yet been described.

Acquired scoliosis poses tremendous challenges across various clinical fields including screening (Fong et al.), prognostication (Robinson and McMaster, 1996) and surgical treatment, with the latter being largely determined by the former two. Prior to diagnosis there is a substantial paucity in early "at-risk" clinical signs which may predict the probability to acquire scoliosis and available screening relies on the clinical (Karachalios et al., 1999) and radiographic (Urrutia et al.) diagnosis of the already deformed spine. In addition, several key clinical and radiographic (Hammond et al.) signs have been suggested to predict the curve's progression rate and final severity once diagnosed. Nevertheless, the absence of an established etiologic mechanism has rendered these signs indirect in nature.

Magnetic resonance imaging (MRI) is a well-established diagnostic tool for neuroimaging and its different imaging contrast techniques are used to study neurological disorders and pathologies. MR findings in the brain of scoliosis patients include increased activation in motor-related cortical areas (Domenech et al.) as well as metabolic abnormalities (Park et al., 2008).

Recently, we have described that a deficiency in a key molecular element essential for the proper development of the entire proprioceptive system, such as *RUNX3* transcription factor, results in an acquired scoliosis in an animal model, mimicking the human condition known as adolescent idiopathic scoliosis (AIS) in several key

characteristics (Blecher et al.). First, the deformity most commonly appeared around sexual puberty (days 40-60 post natal) and progressed at the fastest rate shortly after that period. Second, morphology analysis revealed that scoliosis was not preceded by osseous vertebral anomalies. Finally, the majority of animals developed a right thoracic deformity, also corresponding to the common morphology in humans.

In this work we hypothesize that proprioceptive-deficient Runx3 mutant animal model of acquired scoliosis may serve to explore novel diagnostic and prognostic signs of scoliosis, based on mechanism-specific pre-scoliosis neural anomalies. We show that young pre-scoliosis proprioception-deficient Runx3 mutants possess marked changes in several proprioception-related brain areas detected by magnetic resonance imaging (MRI). These changes were found to be highly correlated with an ensuing scoliosis, but not with its severity, suggesting a possible application of the suggested model in scoliosis screening and diagnosis.

RESULTS

Proprioception deficiency results in acquired peri-pubertal right thoracic scoliosis

We recently reported that proprioception deficiency results in acquired scoliosis which mimics several major characteristics of the human condition known as adolescent idiopathic scoliosis (AIS), thereby suggesting an animal model for the disease. The spinal deformity usually appears around the period of sexual puberty, is unaccompanied by vertebral morphologic anomalies and usually has a right-sided thoracic apex (Figure 1).

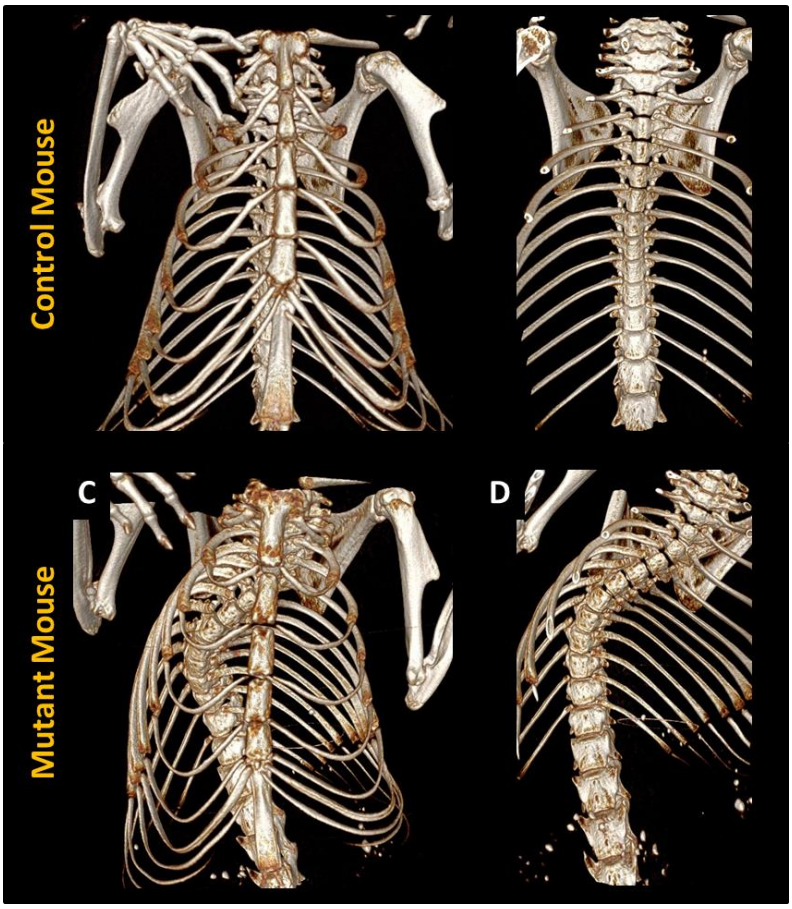

Figure 1**. Runx3 deficiency-related proprioception ablation results in acquired spinal deformity. (A-D)** In-vivo CT scans of mature Runx3 mutant mouse shows

a right-sided thoracic scoliosis distorting the spinal column and adjacent rib cage (C, D). In contrast, the spine of a control littermate is normally aligned (A, B).

Young pre-scoliotic Runx3 KO mice do not display gross morphological brain abnormalities

Having established a role for proprioception in maintaining spinal alignment we explored the possibility that young pre-scoliotic Runx3 mutant animals may display central nervous system (CNS) abnormalities, thereby possibly serving as early markers. For that, we performed in-vivo MRI scans, acquiring T2-weighted coronal images from young (5-7 weeks old) Runx3 mutant animal and compared it to control littermates (Figure 2). Preliminary qualitative analysis showed that T2-weighted MR images of the mutant and control young mice appeared similar. This excluded the possibility of gross morphological or water content differences between brains of mutant and control mice.

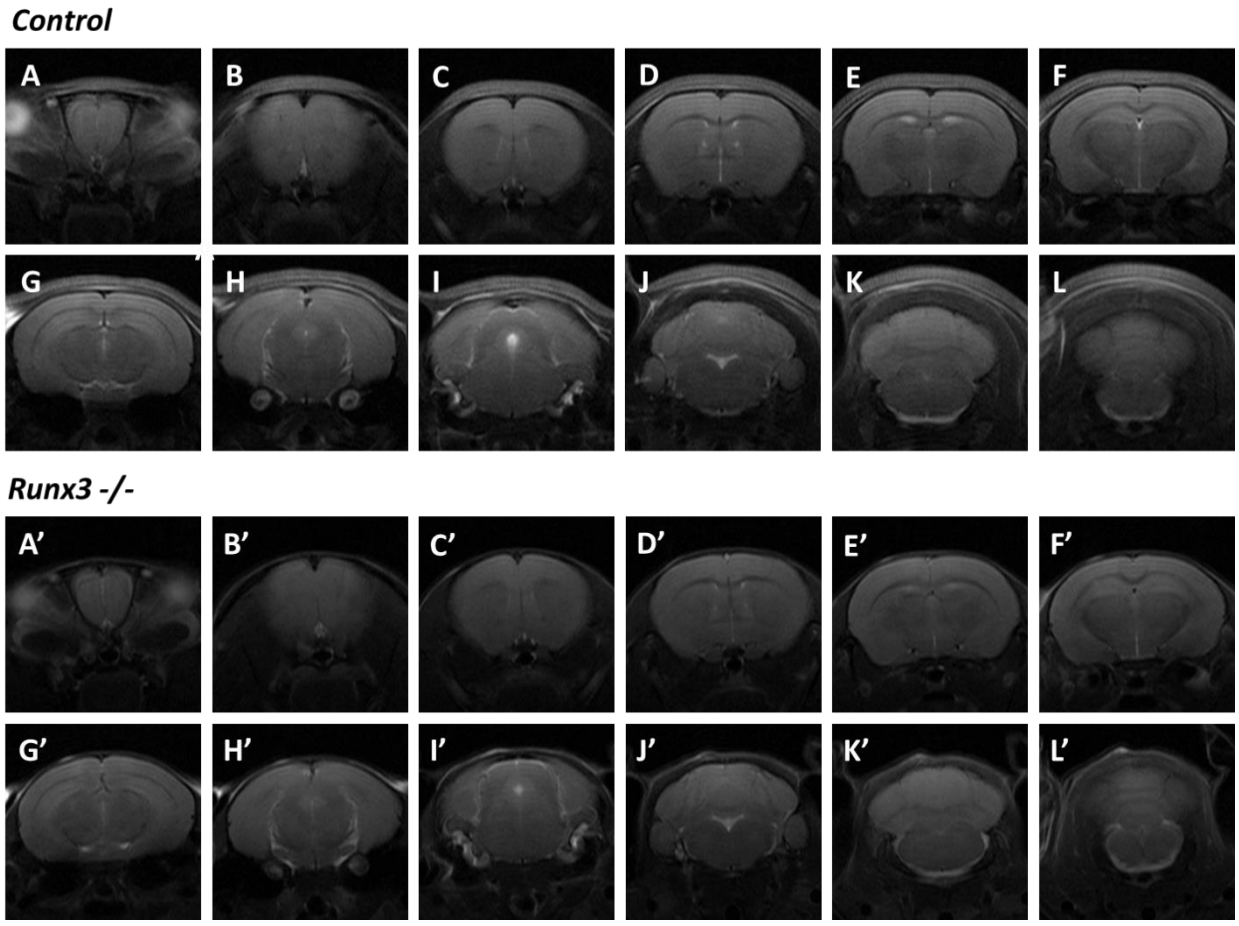

Figure 2. **Runx3 deficient mice do not display gross morphological brain abnormalities (A-L;A'-L').** In-vivo MRI T2 images of coronal sections from anterior to posterior of control (A-L) and Runx3 mutant (A'-L') mice. No gross change in T2 signal is noted between groups, indicating the absence of a gross morphological abnormality.

Young pre-scoliotic Runx3 KO mice have distinct Proprioception-related brain abnormalities detected on magnetic resonance imaging

Next, in order to analyze possible quantitative differences, we acquired T2 brain maps of both groups. This was followed by mouse brain atlas registration and

realignment in order to overcome inter- and intra- group brain size differences. Finally, voxel-by-voxel analysis enabled the statistical analysis and detection of minute T2 signal differences across groups.

Strikingly, Results revealed small but significant ($p<0.01$) abnormalities in several brain areas in the brains of Runx3 mutant mice (Figure 3). Detailed T2 signal comparison between mutants and controls across the various brain areas is presented in table 1.

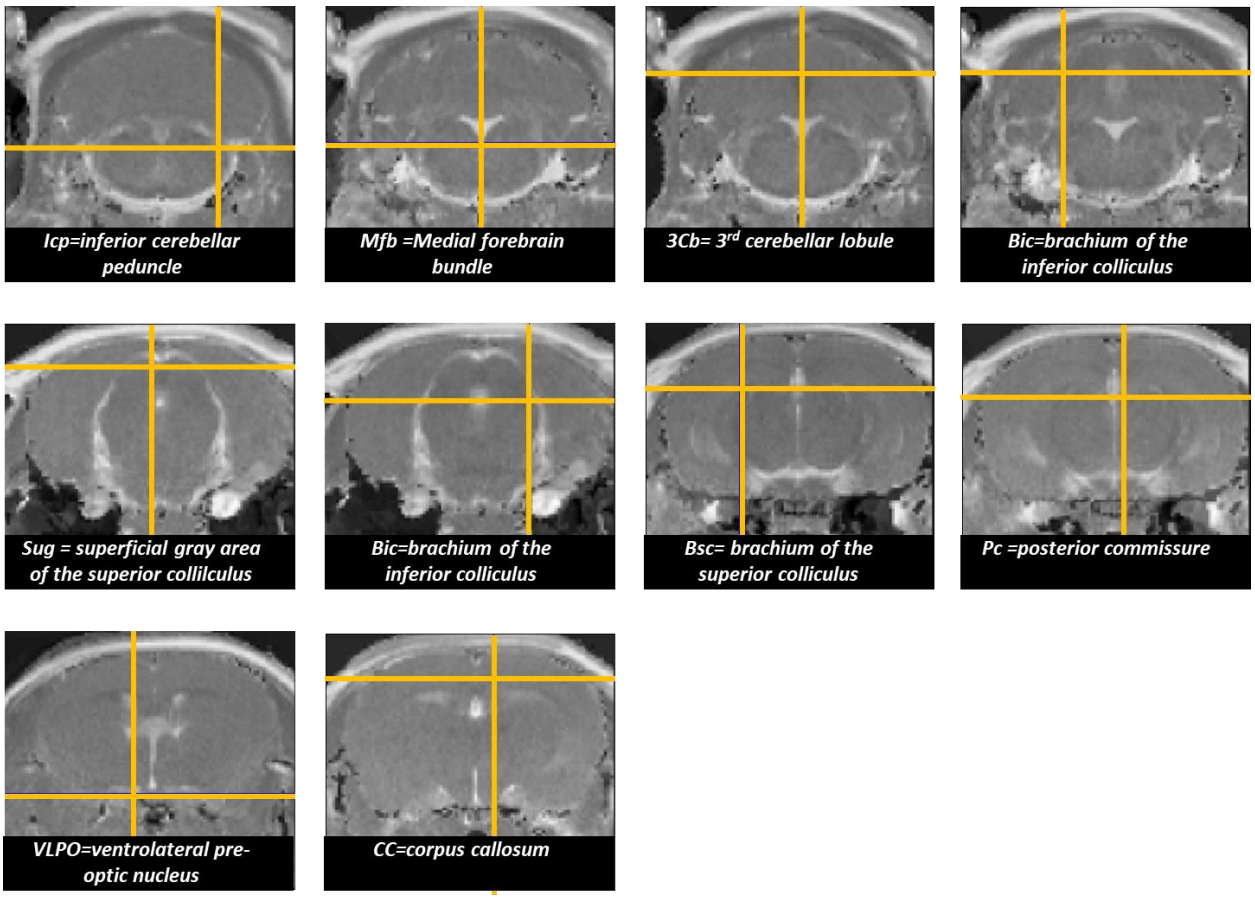

Figure 3. **Runx3 deficiency is associated with increased T2 signal across various brain regions in young animals.** Coronal MRI slices of young Runx3 mutants depicting the various anatomic locations in which T2 signal was found to be significantly increased compared to controls.

Brain Regions	**Wt Mice (NA=7)**	**Mutant Mice (NA=30)**
Inferior cerebellar peduncle (***icp***) *	56.0±7.6 ms	69.7±10.5 ms
Medial forebrain bundle (***mlf***) *	54.0±3.2 ms	66.0±8.3 ms
3rd cerebellar lobule (***3Cb***) *	44.4±3.3 ms	50.8±4.7 ms
Brachium of the inferior colliculus (***bic1***) **	47.1±1.4 ms	54.3±4.8 ms
Superficial gray layer of the superior colliculus (***SuG***) **	45.1±1.1 ms	47.0±2.1 ms
Brachium of the inferior colliculus (***bic2***) **	47.1±0.6 ms	49.9±1.6 ms
Brachium of the superior colliculus (***bsc***) **	47.6±0.5 ms	50.0±1.6 ms
Posterior commissure (**pc**) **	46.9±2.4 ms	54.0±3.5 ms
ventrolateral preoptic nucleus (***VLPO***) *	60.0±4.5 ms	72.8±7.5 ms
Corpus callosum (***cc***) **	45.1±0.7 ms	47.6±1.2 ms

Functional grouping (Figure 4) of young Runx3 mutant brain areas with significant ($p<0.01$) increase in T2 signal identified several key involved brain pathways. The inferior cerebellar peduncle (icp;Figure 4B), which is mainly associated with the integration of proprioceptive sensory input with motor and vestibular inputs, was found to display a 24±15 % increase ($p<0.002$) in the T2 signal compared to controls. Several areas displaying increased T2 signal were also noted to involve the visual pathway (Figure 4D). The tectospinal tracts, for example, (Figure 4C), which begins at the superior colliculus, receives input from the optic nerves and coordinates movements of the head according to vision stimuli. Brain regions along this tract include the superficial gray layer of the superior colliculus (SuG)

and brachium of the superior colliculus (bsc). Other visual-related areas included the ventrolateral preoptic nucleus and posterior commissure. Finally, areas associated with motor control such as the corpus callosum and the cerebellum displayed similarly significantly increased T2 signal.

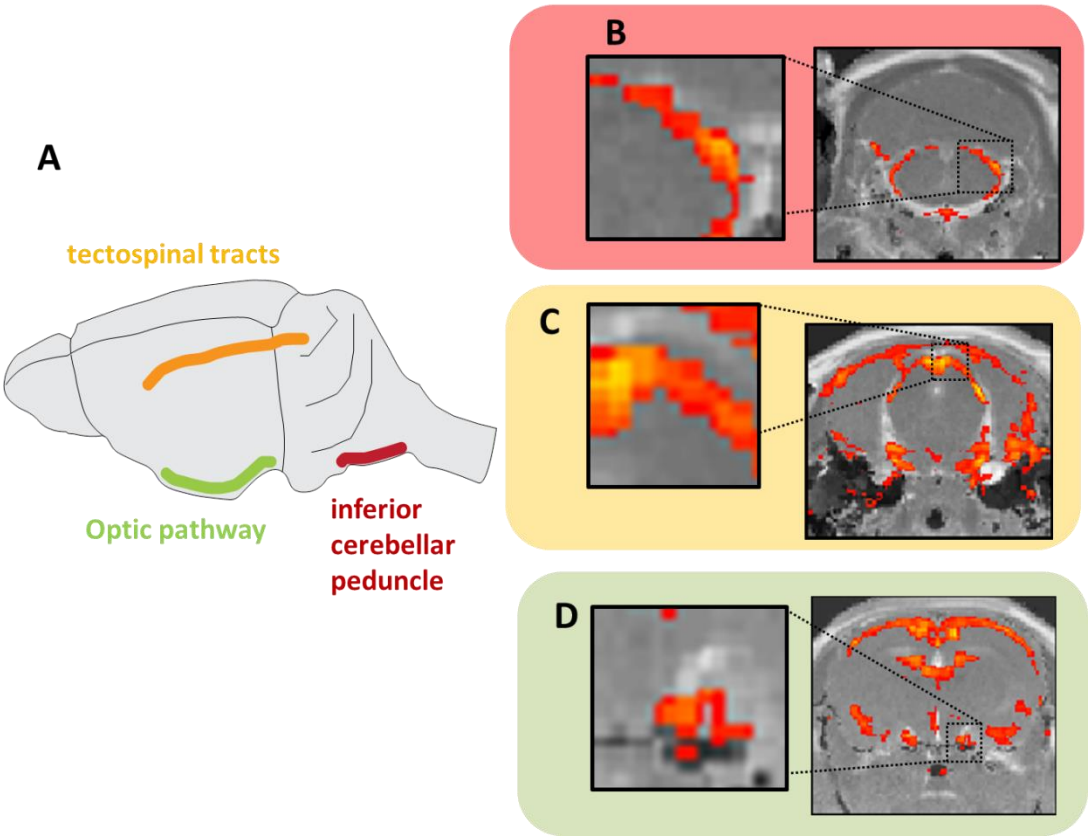

Figure 4. **Runx3 mutants display increased T2 signals along three major brain tracts (A-D).** In vivo MRI showing three representative coronal slices of T2-weighted images and magnification of selected areas (B-D). Areas in mutants which displayed significant increased T2 signal are represented by red-yellow dots (yellow shift represents higher significance). Associated areas were found to involve the inferior cerebellar peduncle (B), tectospinal tracts (C) and the optic pathways (D).

Brain anomalies in young Runx3 mutants predict both mild as well as severe spinal deformities

Having proposed possible early diagnostic markers for developing scoliosis in proprioceptive-deficient animal model, we sought to explore a possible prognostic role which may indicate the final curve severity. For that we CT scanned the same Runx3 mutants at the age of 3 months and analyzed the severity of the major curve using the standard Cobb angle measurement. As expected, in contrast to controls, the majority of mature Runx3 mutant animals displayed substantial right thoracic curves, ranging from 4 to 76 degrees (Figure 5). For the purpose of statistical analysis we divided the group of Runx3 mutants (n=30) into 2, grading final curves as being moderate (grade 0: less than 30 degrees; n=15) or severe (grade 0: less than 30 degrees; n=15)

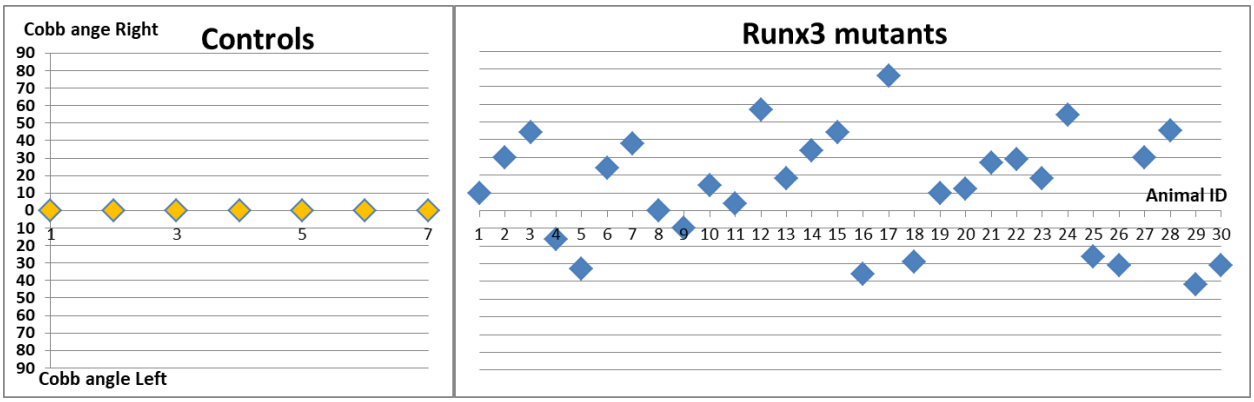

Figure 5. **Runx3 deficiency results in acquired spinal deformity in adulthood**. As previously reported, Runx3 mutants develop new onset spinal deformity with the majority of major curves being right sided thoracic.

Next, to assess whether T2 signal in young animals may predict curve severity in maturity we compared the average T2 signal between grades 0 and 1 of curve severity in adult mutants across the various brain regions. Statistical analysis

showed that average T2 signal did not differ significantly across the various key (Figure 6).

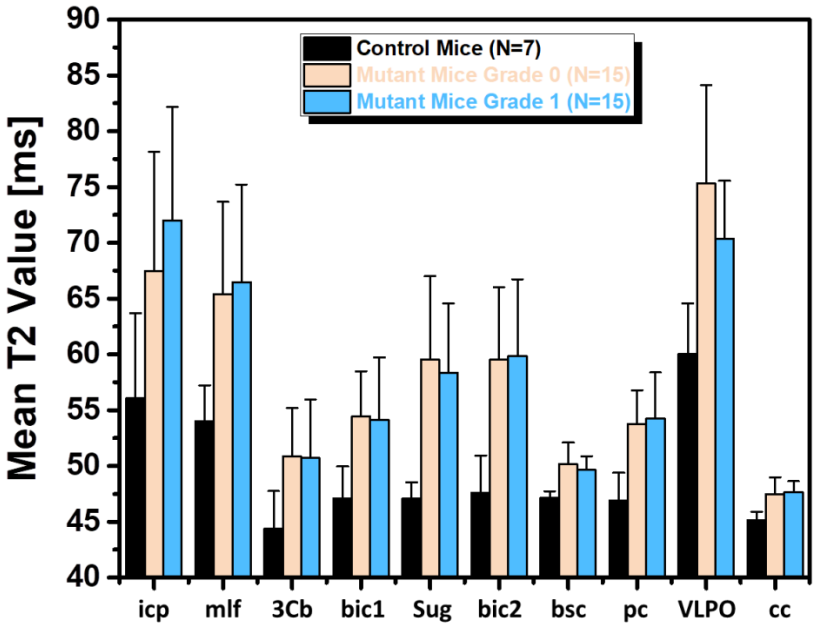

Figure 6. **Average T2 signal in young Runx3 mutants does not correlate with curve severity in maturity.** Bars indicating average T2 signal in young animals of three groups: controls (black), Runx3 mutants that acquired moderate curves at maturity (Pink) and Runx3 mutants that acquired severe curves at maturity (blue). Although a marked difference is noted between controls and mutants, final curve severity did not seem to correlate with early T2 signal average.

DISCUSSION

In spite of continuing effort, the causative mechanism of Adolescent idiopathic scoliosis (AIS) has remained obscure. The attempts to decipher its pathogenesis have focused on several research strategies. On the anatomic level, numerous tissues have been suggested to presumably be involved with AIS pathogenesis including connective tissue, muscular (Acaroglu et al., 2009; McIntire et al., 2007), neural and neuroendocrine (Machida et al., 1995). A debate, however on whether identified changes represent a primary or a secondary change has remained unanswered. Various attempts have also been made to suggest an animal model compatible with AIS (Pal et al., 1991; Pincott et al., 1984; Robin, 1996). Nonetheless, the absence in a model that closely recapitulates the condition's dynamic and unique characteristics has resulted in a relatively lack of a single acceptable animal model.

Interestingly, proprioception dysfunction has long been suggested to play a role in AIS pathogenesis. Indirect supporting evidence have emerged from various research endeavors. In the study of AIS patient tissue and function abnormalities, studies have identified abnormal muscle spindle number and function (Ford et al., 1988), altered gait and balance (Guo et al., 2006) as well as impairment in proprioceptive-specific tasks (Yekutiel et al., 1981).

In a recently published work, we supplied with an animal model which strengthens proprioception dysfunction as a possible underlying mechanism for AIS (Blecher et al.). Animals lacking key molecular players essential for proprioception system's assembly developed acquired right thoracic scoliosis in the absence of vertebral anomalies.

In this work we have elaborated on possible other neural manifestation which characterize the main strain used in our previous study, the Runx3 mutant. Focusing on the brain of Runx3 deficient animal prior to acquiring scoliosis has enabled the analysis of possible pre-scoliosis markers in the attempt to possibly improve future AIS diagnosis. We show that young Runx3 mutants deficient in proprioception also possess significant brain anomalies prior to the acquisition of scoliosis, thereby serving as anatomic areas of possible diagnostic value. The identity of involved brain areas which include motor, visual and proprioceptive specific tracts further strengthen the hypothesis that observed abnormalities are secondary to the primary proprioception peripheral insult. Moreover, MRI studies on AIS patients which identified anomalies in similar brain areas including the cerebellum and corpus callosum further strengthen our findings (Schlosser et al., ; Shi et al., 2013).

Nevertheless, this study is marked by several limitations. We have not shown the anatomic nature of the brain areas in which T2 signal was found to be increased. In a preliminary histologic study, we were unable to identify gross alteration in the myelination or evidence of inflammation involving the brain areas. In addition, the question of whether Runx3 deficiency results in brain anomalies in a proprioceptive –mediated effect or through other non-neural effect has remained unanswered.

To conclude, we believe that the data presented is valuable in the attempt to advance AIS research as it provides important candidate anatomic regions which may be utilized in the development of better future diagnostic tests.

Methods

MRI

Animal experiments were approved by the Weizmann institute Animal Care and Use Committee Following US National Institute of Health, European Commission and the Israeli guidelines. Brain MRI measurements were performed at two time points (as young mice: 3-4 weeks and as adult mice: 3-4 months). During the MRI scanning, mice were anesthetized with Isofluorane (5% for induction, 1–2% for maintenance) mixed with oxygen (1 liter/min) and delivered through a nasal mask. Once anesthetized, the animals were placed in a head-holder to assure reproducible positioning inside the magnet. Respiration rate was monitored and kept throughout the experimental period around 60–80 breaths per minute.

MRI experiments were performed on 9.4 Tesla BioSpec Magnet 94/20 USR system (Bruker, Germany) equipped with gradient coil system capable of producing pulse gradient of up to 40 gauss/cm in each of the three directions. All MR images had been acquired with a receive quadrature mouse head surface coil and transmitter linear coil (Bruker). The T2 maps were acquired using the multi-slice spin-echo (MSME) imaging sequence with the following parameters: a repetition delay (TR) of 3000 ms, 16 time echo (TE) increments (linearly from 10 to 160ms), matrix dimension of 256 x 128 (interpolated to 256 x 256) and two averages, corresponding to an image acquisition time of 12min 48sec. The T2 dataset consisted of 16 images per slice. Thirteen continuous slices with slice thickness of 1.00 mm were acquired with a field of view (FOV) of 2.0 x 2.0 cm2.

Image Analysis

A quantitative T2 map was produced from multi-echo T2-weighted images. The multi-echo signal was fitted to a mono-exponential decay to extract the T2 value for each image pixel. All image analysis was performed using homemade scripts written in Matlab R2013B. Co-registration inter-subject and intra-subject was applied before the MRI dataset analysis. For optimal suitability to a mouse brain atlas (correction of head movements image artifacts), all images went through atlas registration: reslicing, realignment and smoothing, using the SPM software (version 12, UCL, London, UK).

Statistical Methods

The results were reported as mean ± SD. A t-test was used to compare means of two groups. A p value of less than 0.05 was considered statistically significant.

CT

Prior Micro-CT scanning the mice were anesthetized using IM injection of a mix of Domitor (Medetomidine, 1mg/Kg) and Ketamine (75mg/Kg). At the end of the MRI protocol, the anesthetized chameleon will be injected with IP injection of Antisedan (1mg/kg). The mice were scanned using a micro-CT device TomoScope ® 30S Duo scanner (CT Imaging, Germany) equipped with two source-detector systems. The scanner uses two x-ray sources and a detector system that are mounted on a gantry that rotates around a bed holding the animal. The operation voltages of both tubes were 40kV. The integration time of protocols was 90ms (360 rotations) for 3cm length and axial images were obtained at an isotropic resolution of 80μ. Due to the maximum length limit, to cover the whole mouse body, imaging was performed in two-four parts with overlapping area and then all slices merged to one dataset representing the entire ROI. The radiation dose range was 2.1-4.2Gy.

All micro-CT scans were reconstructed using a filtered back-projection algorithm using scanner software. Then the reconstructed data sets for each rat were merged to one data set using ImageJ software. 3D volume rendering images were produced using Amira Software.

References

Acaroglu, E., Akel, I., Alanay, A., Yazici, M., and Marcucio, R. (2009). Comparison of the melatonin and calmodulin in paravertebral muscle and platelets of patients with or without adolescent idiopathic scoliosis. Spine *34*, E659-663.

Blecher, R., Krief, S., Galili, T., Biton, I.E., Stern, T., Assaraf, E., Levanon, D., Appel, E., Anekstein, Y., Agar, G.*, et al.* The Proprioceptive System Masterminds Spinal Alignment: Insight into the Mechanism of Scoliosis. Developmental cell *42*, 388-399 e383.

Domenech, J., Garcia-Marti, G., Marti-Bonmati, L., Barrios, C., Tormos, J.M., and Pascual-Leone, A. Abnormal activation of the motor cortical network in idiopathic scoliosis demonstrated by functional MRI. Eur Spine J *20*, 1069-1078.

Fong, D.Y., Cheung, K.M., Wong, Y.W., Wan, Y.Y., Lee, C.F., Lam, T.P., Cheng, J.C., Ng, B.K., and Luk, K.D. A population-based cohort study of 394,401 children followed for 10 years exhibits sustained effectiveness of scoliosis screening. Spine J *15*, 825-833.

Ford, D.M., Bagnall, K.M., Clements, C.A., and McFadden, K.D. (1988). Muscle spindles in the paraspinal musculature of patients with adolescent idiopathic scoliosis. Spine (Phila Pa 1976) *13*, 461-465.

Guo, X., Chau, W.W., Hui-Chan, C.W., Cheung, C.S., Tsang, W.W., and Cheng, J.C. (2006). Balance control in adolescents with idiopathic scoliosis and disturbed somatosensory function. Spine (Phila Pa 1976) *31*, E437-440.

Hammond, K.E., Dierckman, B.D., Burnworth, L., Meehan, P.L., and Oswald, T.S. Inter-observer and intra-observer reliability of the Risser sign in a metropolitan scoliosis screening program. J Pediatr Orthop *31*, e80-84.
Karachalios, T., Sofianos, J., Roidis, N., Sapkas, G., Korres, D., and Nikolopoulos, K. (1999). Ten-year follow-up evaluation of a school screening program for scoliosis. Is the forward-bending test an accurate diagnostic criterion for the screening of scoliosis? Spine *24*, 2318-2324.
Machida, M., Dubousset, J., Imamura, Y., Iwaya, T., Yamada, T., and Kimura, J. (1995). Role of melatonin deficiency in the development of scoliosis in pinealectomised chickens. J Bone Joint Surg Br *77*, 134-138.
McIntire, K.L., Asher, M.A., Burton, D.C., and Liu, W. (2007). Trunk rotational strength asymmetry in adolescents with idiopathic scoliosis: an observational study. Scoliosis *2*, 9.
Pal, G.P., Bhatt, R.H., and Patel, V.S. (1991). Mechanism of production of experimental scoliosis in rabbits. Spine (Phila Pa 1976) *16*, 137-142.
Park, W.W., Suh, K.T., Kim, J.I., Ku, J.G., Lee, H.S., Kim, S.J., Kim, I.J., Kim, Y.K., and Lee, J.S. (2008). Cerebral glucose metabolic abnormality in patients with congenital scoliosis. Eur Spine J *17*, 948-955.
Pincott, J.R., Davies, J.S., and Taffs, L.F. (1984). Scoliosis caused by section of dorsal spinal nerve roots. J Bone Joint Surg Br *66*, 27-29.
Robin, G.C. (1996). Scoliosis induced by rib resection in chickens. J Spinal Disord *9*, 351.
Robinson, C.M., and McMaster, M.J. (1996). Juvenile idiopathic scoliosis. Curve patterns and prognosis in one hundred and nine patients. The Journal of bone and joint surgery *78*, 1140-1148.
Schlosser, T.P., van der Heijden, G.J., Versteeg, A.L., and Castelein, R.M. How 'idiopathic' is adolescent idiopathic scoliosis? A systematic review on associated abnormalities. PLoS One *9*, e97461.
Shi, L., Wang, D., Hui, S.C., Tong, M.C., Cheng, J.C., and Chu, W.C. (2013). Volumetric changes in cerebellar regions in adolescent idiopathic scoliosis compared with healthy controls. Spine J *13*, 1904-1911.
SRS (2016). Adolescent Idiopathic Scoliosis (Scoliosis Research Society).
Urrutia, J., Besa, P., and Bengoa, F. A prevalence study of thoracic scoliosis in Chilean patients aged 10-20 years using chest radiographs as a screening tool. Journal of pediatric orthopedics.
Yekutiel, M., Robin, G.C., and Yarom, R. (1981). Proprioceptive function in children with adolescent idiopathic scoliosis. Spine *6*, 560-566.